BULLETIN OF THE POLISH ACADEMY OF SCIENCES
TECHNICAL SCIENCES, Vol. 68, No. 5, 2020
DOI: 10.24425/bpasts.2020.134647

Predictive-SVM control method dedicated to an AC/DC converter with an LCL grid filter

K. DMITRUK*

Bialystok University of Technology, Electric Engineering Faculty, Department of Power Electronics and Electric Drives

Abstract. This paper presents simulation and laboratory test results of an implementation of an infinite control set model predictive control into a three-phase AC/DC converter. The connection between the converter and electric grid is made through an LCL filter, which is characterized by a better reduction of grid current distortions and smaller (cheaper) components in comparison to an L-type filter. On the other hand, this type of filter can cause strong resonance at specific current harmonics, which is efficiently suppressed by the control strategy focusing on the strict control input filter capacitors voltage vector. The presented method links the benefits of using linear control methods based on a space vector modulator and the nonlinear ones, which result in excellent control performance in a steady state as well as in a transient state.

Key words: three-phase voltage converter, model predictive control, space vector modulation, infinite control set.

1. Introduction

The multi-directional and dynamic development of material, information, and production technologies enables us to use renewable energy sources more efficiently. Many experts focus on improving the first stage of electricity conversion associated with obtaining it directly from solar, wind, or water energy. Subsequently, the acquired energy is transferred to the converter's DC-link via DC or AC voltage converter, depending on the type of energy source. Then, using the AC/DC converter, it is transformed and pushed into the power grid. A large number of renewable energy sources in the electricity grid have their advantages. By increasing local electricity resources, the reliability of powering energy consumers is improved [1, 2]. However, the operation of power electronics devices has an impact on the quality of electricity [3, 4]. Switching the transistors in the converter branches results in higher harmonics, which reduces the efficiency of the power electronics device itself and also increases transmission losses in the power network [5–7]. This forces us to use larger filters connected between the converter and the power grid. The simplest method of filtration is the use of an L-type filter. An example diagram of the converter coupled to the power grid through an L filter is shown in Fig. 1.

This method of combining the converter with the power supply network offers numerous advantages. These include the absence of a resonant frequency of the filter and the ease of use with most of the converters control methods (linear and nonlinear) [8, 9]. However, for effective filtration, a higher inductance value should be used, especially when compared to the total inductance characterizing LCL type filters offering the same suppression efficiency of higher harmonics [10, 11].

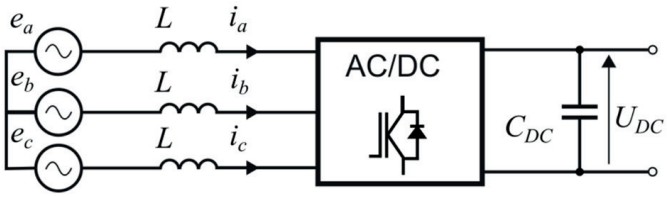

Fig. 1. Connection diagram of the converter to the power grid using an L-filter

Considering an exemplary diagram of the converter connected to the power supply via an LCL filter (Fig. 2), we notice two resonant circuits. The first of them consists of elements L_1 and C, and the second of elements L_2 and C. In order to achieve high quality of the grid current regulation, appropriate resonance frequencies should be ensured during the design phase of the filter, which will not amplify the harmonics generated by an AC/DC converter.

For this reason, nonlinear control methods with variable switching frequency [12–15] are problematic when used in the system from Fig. 2. Therefore, this article presents a new, predictive AC/DC converter control method with an infinite number of converter output voltage vectors.

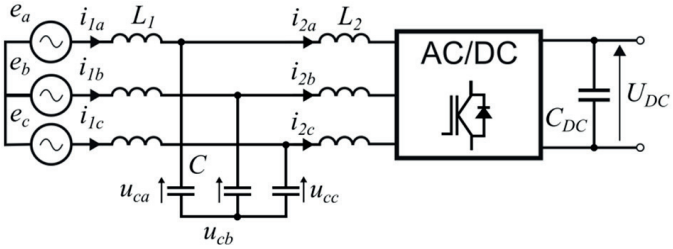

Fig. 2. Connection diagram of the converter to the power grid using an LCL filter

*e-mail: k.dmitruk@pb.edu.pl

Manuscript submitted 2020-01-09, revised 2020-03-24, initially accepted for publication 2020-03-31, published in October 2020

This method aims to minimize higher harmonics introduced into the power supply network by using Space Vector Modulation (SVM). This results in a constant switching frequency, which facilitates filtering the unwanted current components. The general principle of the presented control algorithm is based on controlling voltage on the filter capacitance. It allows the reduction of resonant harmonics and obtaining a sinusoidal grid current.

In the literature, other methods use SVM to control the converter connected to the power supply via an LCL filter. An example is stated in Zhang et al. 2018 [16], where the predictive method was used but the control structure utilises additional feedback from the capacitor current simulating damping resistance, which the proposed control method does not exhibit. Another example of control is the use of a combination of linear and resonant controllers in the control loop [17]. In the abovementioned article, the quality of the generated current is lower compared to the proposed control method despite the use of higher filter inductances and the same switching frequency.

The remaining contents of the paper are organized as follows: in Section 2 the mathematical model of the grid-connected converter system is analysed, followed by the explanation of the proposed control strategy in Section 3. Section 4 introduces the simulation results, and section 5 presents the experimental results to show the efficiency of the proposed method. Finally, Section 6 concludes this paper.

2. Considered model

All operations related to the control system are performed in a rotating *xy* reference frame. The considered model of an LCL type filter is shown in Fig. 3.

The filter consists of the inductance L_1 on the network side, the inductance L_2 on the converter side, and the filtering capacitor C. On the right side of the figure, the discrete nature of the voltage variations $\boldsymbol{u}_2$ on the converter AC terminals is marked. The following equations describing the dependencies between

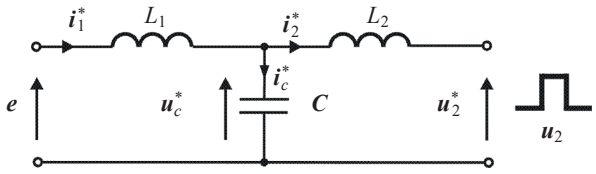

Fig. 3. Diagram of an LCL filter coupling the power supply network with the converter in a rotating reference frame *xy*

voltages and currents in an LCL filter were used for the synthesis of control rules:

$$L_1 \frac{d}{dt}\boldsymbol{i}_1 = \boldsymbol{e} - j\omega_g L_1 \boldsymbol{i}_1^* - \boldsymbol{u}_c = \boldsymbol{u}_c^* - \boldsymbol{u}_S, \tag{1}$$

$$L_2 \frac{d}{dt}\boldsymbol{i}_2 = \boldsymbol{u}_c - j\omega_g L_2 \boldsymbol{i}_2^* - \boldsymbol{u}_2 = \boldsymbol{u}_2^* - \boldsymbol{u}_2, \tag{2}$$

$$C \frac{d}{dt}\boldsymbol{u}_c = \boldsymbol{i}_1 - \boldsymbol{i}_2 - j\omega_g C \boldsymbol{u}_c, \tag{3}$$

where

$\boldsymbol{e}$ – grid voltage vector,
$\boldsymbol{u}_c$ – capacitor voltage vector in the LCL filter,
$\boldsymbol{u}_2$ – converter voltage vector,
$\boldsymbol{i}_1$ – grid current vector,
$\boldsymbol{i}_2$ – inverter current vector,
L_1 – filter inductance on the grid side,
L_2 – filter inductance on the converter side,
C – capacitance of the filter capacitors,
ω_g – grid pulsation.

All variables marked by "*" represent set values of voltages or currents.

3. Control circuit

Figure 4 shows the overall structure of the proposed control system, which is oriented to the power grid voltage vector $\boldsymbol{e}$.

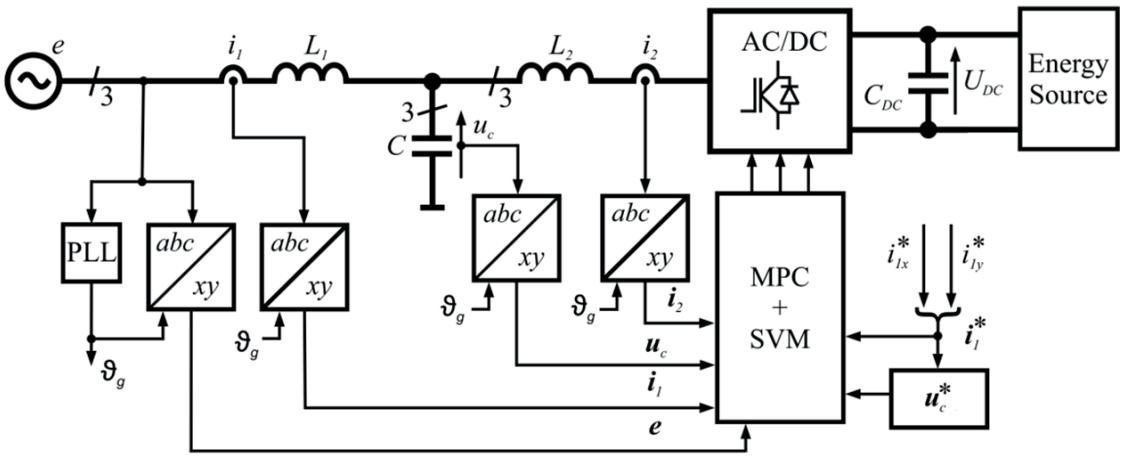

Fig. 4. Structure of the control system

The converter side current $\boldsymbol{i}_2$ is formed by the difference between the filter capacitor voltage $\boldsymbol{u}_c$ and the voltage at the AC terminals of the converter $\boldsymbol{u}_2$. The output voltage of the converter varies considerably faster than the capacitor voltage. Hence, it is assumed that during one control period, the voltage vectors generated by the converter have a significant impact on the current changes in inductance L_2. The tested system uses a two-level converter, which generates six active and two zero vectors on the AC terminals (4).

$$\boldsymbol{u}_2 = \begin{cases} \frac{2}{3} U_{dc} e^{j(n-1)(\pi/3)} & for\ n = \{1, 2, 3, 4, 5, 6\} \\ \text{'0'} & for\ n = \{0, 7\} \end{cases} \tag{4}$$

The vectors described above are shown in Fig. 5. In addition, the figure presents a vector interpretation of the equations describing the dependencies occurring in an LCL filter (1–3). The voltage derivatives $\boldsymbol{d}_{2u'xxx'}$ visible in the drawing are defined as the difference between the set voltage $\boldsymbol{u}_2^*$ and the available voltage vectors $\boldsymbol{u}_2$.

From (2) and (4), a quantity $\boldsymbol{d}_{2u}$ proportional to the converter current derivative scaled by factor L_2 is calculated:

$$L_2 \frac{d}{dt} \boldsymbol{i}_2 = \boldsymbol{u}_2^* - \boldsymbol{u}_2 = \boldsymbol{d}_{2u}, \tag{5}$$

where

$$\boldsymbol{u}_2^* = \boldsymbol{u}_c^* - \boldsymbol{i}_2^* j\omega_g L_2, \tag{6}$$

and the voltage setpoint on the filter capacitor $\boldsymbol{u}_c^*$:

$$\boldsymbol{u}_c^* = \boldsymbol{e} - \boldsymbol{i}_1^* j\omega_g L_1. \tag{7}$$

Switching on any voltage vector $\boldsymbol{u}_2$ changes the current vector $\boldsymbol{i}_2$. The direction of changes in the vector $\boldsymbol{i}_2$ position can be calculated from the vector $\boldsymbol{d}_{2u}$:

$$\boldsymbol{d}_{2i} = \frac{d}{dt} \boldsymbol{i}_2 = \boldsymbol{d}_{2u} / L_2. \tag{8}$$

The predicted position of the converter current vector $\boldsymbol{i}_2$ after using the selected vector $\boldsymbol{u}_2$ for time T_s:

$$\boldsymbol{i}_{2p} + \boldsymbol{i}_2 = \boldsymbol{d}_{2i} T_s. \tag{9}$$

The maximum displacement of the $\boldsymbol{i}_2$ vector depends on the selected converter voltage vector, the sampling time of the control system T_s and the inductance L_2. Figure 6 graphically illustrates the possibilities of controlling the $\boldsymbol{i}_2$ vector.

After determining the new position of the converter current vector ($\boldsymbol{i}_{2p}$), it is possible to define the direction of changes $\boldsymbol{d}_{uc}$ of the voltage vector on the filter capacitor:

$$\boldsymbol{d}_{uc} = \frac{d}{dt}(\boldsymbol{u}_c) = \frac{\boldsymbol{i}_1 - \boldsymbol{i}_{2p} - j\omega_g C \boldsymbol{u}_c^*}{C}. \tag{10}$$

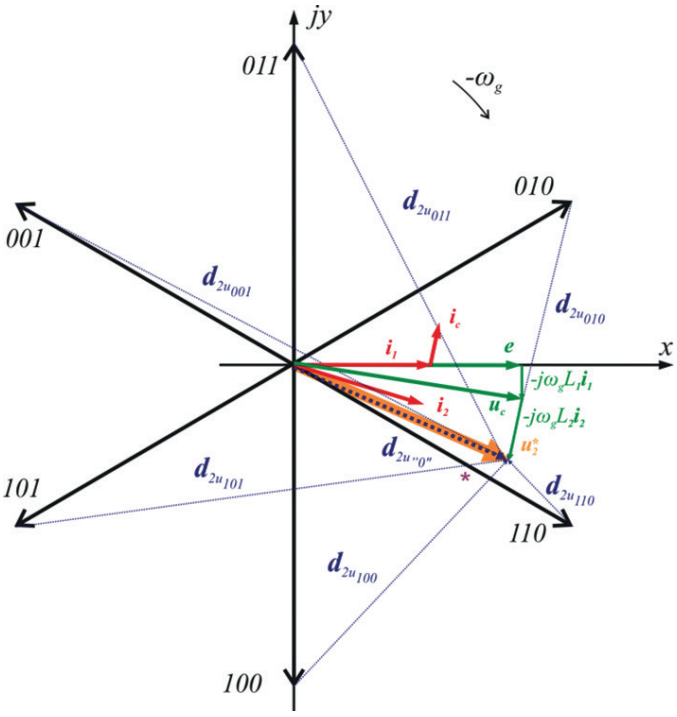

Fig. 5. Available vectors on AC terminals of a two-level converter and graphic interpretation of equations describing voltages and currents in an LCL filter

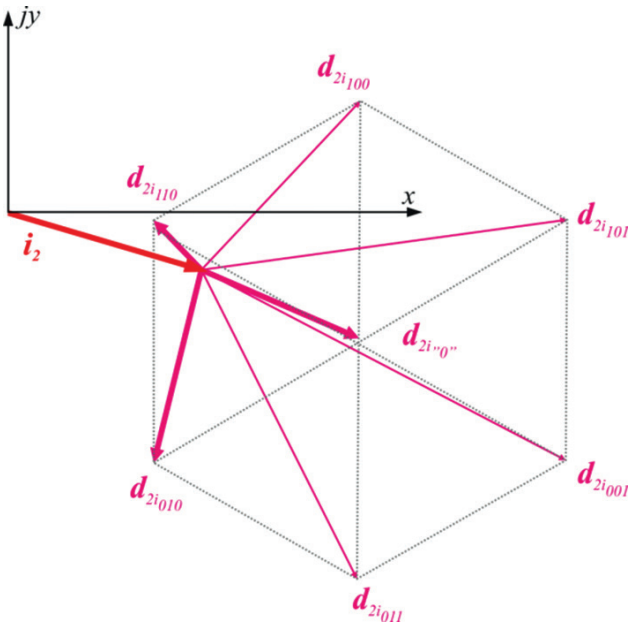

Fig. 6. Available displacements of the end position of the converter current vector ($\boldsymbol{i}_{2xy}$) during one control period

Predicted voltage vector on the filter capacitor $\boldsymbol{u}_{cp}$ changes their position due to the converter current vector position displacement. After time T_s, a new position of that vector is:

$$\boldsymbol{u}_{cp} = \boldsymbol{u}_c + \boldsymbol{d}_{uc} T_s. \tag{11}$$

Similarly, to determining the changes of the $\boldsymbol{i}_2$ vector due to the interaction of the converter vectors $\boldsymbol{u}_2$, the changes of the $\boldsymbol{i}_1$ vector are determined based on the voltage changes on the filter capacitor. It is assumed that the voltage value $\boldsymbol{u}_c$ on the filter capacitor changes significantly faster than the voltage value in the supply network as a result of the interaction of the converter voltage vectors. This is described by the following equations:

$$L_1 \frac{d}{dt} \boldsymbol{i}_1 = \boldsymbol{u}_c - \boldsymbol{u}_{cp} = \boldsymbol{d}_{1u}, \tag{12}$$

$$\boldsymbol{d}_{1i} = \frac{d}{dt} \boldsymbol{i}_1 = \boldsymbol{d}_{1u}/L_1, \tag{13}$$

$$\boldsymbol{i}_{1p} = \boldsymbol{i}_1 + \boldsymbol{d}_{1i} T_s, \tag{14}$$

where

$\boldsymbol{d}_{1u}$ – quantity proportional to grid current derivative,

$\boldsymbol{d}_{1i}$ – quantity describing direction of changes in current vector $\boldsymbol{i}_1$,

$\boldsymbol{i}_{1p}$ – predicted grid current vector position as a result of changing filter capacitor voltage vector.

The equations (5–14) present the principles of voltage and current prediction in an LCL filter as a response to the use of a single vector during one control period. This is a characteristic feature of nonlinear methods from the group of finite control methods (FCS). Control methods from the indicated group are characterized by two main disadvantages. First, they have limited error correction capabilities, which means that it is not possible to achieve zero error after a single control step most of the time. Secondly, they have a variable connection frequency, which makes it challenging to select the value of filter components connecting the converter with the power supply network.

The proposed method is based on "the reverse order" of the analysis equations (5–14). This allows us to determine the exact change in the current $\boldsymbol{i}_2$ on the basis of the value of the current error $\boldsymbol{i}_1$, which will zero the grid current error $\Delta\boldsymbol{i}_1$ during a single control period T_s, at least in theory. The equations presented below were derived from previous relationships and given in the form of differential equations.

Based on the set values of the grid current vector $\boldsymbol{i}_1^*$ and the actual value of the grid current $\boldsymbol{i}_1$ flowing through inductance L_1, the grid current error $\Delta\boldsymbol{i}_1$ is calculated. Equation (15) is based on the transformation of (12–14). In those equations, the $\boldsymbol{i}_{1p}$ vector is replaced by a set value vector of grid current $\boldsymbol{i}_1^*$:

$$\Delta\boldsymbol{i}_1 = \boldsymbol{i}_1^* - \boldsymbol{i}_1 \tag{15}$$

In the next step, the required voltage gain on the LCL filter capacitors is calculated. According to (10) and (11), the error vector $\Delta\boldsymbol{i}_1$ is compensated during the next control period when the capacitor voltage will change the value by $\Delta\boldsymbol{u}_c$.

$$\Delta\boldsymbol{u}_c = \boldsymbol{u}_c^* - \boldsymbol{u}_c - \Delta\boldsymbol{i}_1 L_1/T_s. \tag{16}$$

In order to change the voltage on the filter capacitor, the converter current increase $\Delta\boldsymbol{i}_2$ flowing through the inductance L_2 has to be computed. It is possible by the following equation based on (5, 8 and 9):

$$\Delta\boldsymbol{i}_2 = \boldsymbol{i}_1 - \boldsymbol{i}_2 - j\omega_g C\boldsymbol{u}_c^* - \Delta\boldsymbol{u}_c \cdot C/T_s \tag{17}$$

To reproduce the calculated displacement of the $\boldsymbol{i}_2$ current vector to any point in the hexagon shown in Fig. 7, three-vector modulation during a single control period is used. Such a feature assigns the proposed method to the continuous control set (infinite control set) group of voltage converters control methods.

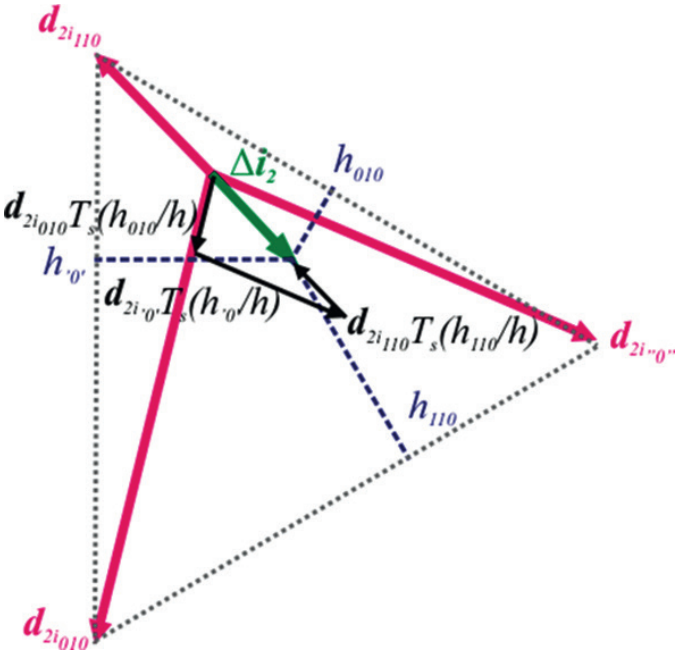

Fig. 7. The method of determining the heights that are the basis for calculating the duties to an SVM modulator in a static state

The most important feature of the proposed algorithm is the use of two approaches to select the generated voltage converter vector depending on the position of the tail of the current error vector $\Delta\boldsymbol{i}_2$. In the event that the error vector $\Delta\boldsymbol{i}_2$ is in the area of the sector where the head of the $\boldsymbol{i}_2$ current vector is located (as in Fig. 7), three-vector modulation is used.

The two shortest voltage derivatives $\boldsymbol{d}_{2u'xxx'}$ and corresponding current derivatives $\boldsymbol{d}_{2u'xxx'}$ (8) choose the two active vectors. The use of the indicated vectors with a zero vector during a single control period creates the $\boldsymbol{i}_{2xy}$ vector, whose tail can be placed in every point of the sector created by the derivative vector tails (Fig. 7). This is done practically by changing the time of use of these vectors during one control period.

The calculation of the duty cycles for an SVM modulator is based on the analysis of the ratio of the height of the vector $\Delta\boldsymbol{i}_2$ head from the sector sides, to the total height of the sector h. A graphic interpretation of the duty cycles calculation method

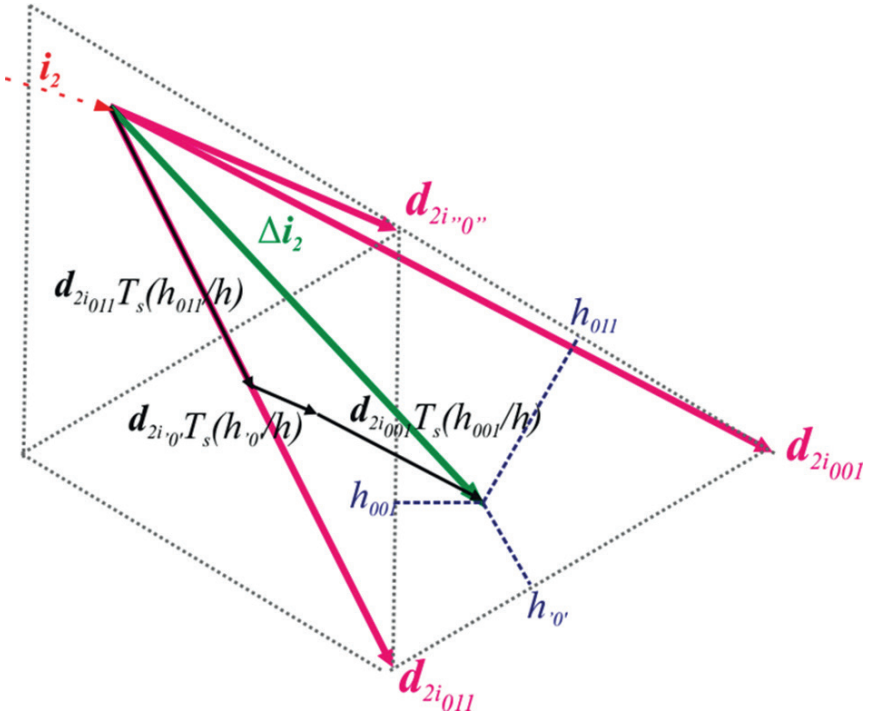

Fig. 8. Selection of converter voltage vectors used in three-vector modulation in case the head of the error vector is another sector than its tail

is illustrated in Fig. 7. Duty cycles are computed using the following equations:

$$dt_A = \frac{V_{(1)Axx}h_1 + V_{(2)Axx}h_2}{h} + \frac{V_{'0'Axx}h_0 + V_{'1'Axxx}h_0}{2h}, \quad (18)$$

$$dt_B = \frac{V_{(1)xBx}h_1 + V_{(2)xBx}h_2}{h} + \frac{V_{'0'xBx}h_0 + V_{'1'xBx}h_0}{2h}, \quad (19)$$

$$dt_C = \frac{V_{(1)xxC}h_1 + V_{(2)xxC}h_2}{h} + \frac{V_{'0'xxC}h_0 + V_{'1'xxC}h_0}{2h}, \quad (20)$$

where $V_{(y)xxx}$ is a one voltage vector from a vector set selected to modulation. Subscript y indicates a number of active vectors in the selected vector set. For example, $V_{(1)xBx}$ from vector 101 is equal to 0, and $V_{(1)xxC}$ is equal to 1. $V_{'0'}$ and $V_{'1'}$ are zero vectors. A precise description of calculating those duty cycles is presented in [18].

If the head of the error vector $\Delta\boldsymbol{i}_2$ is placed inside another sector than the head of the current vector $\boldsymbol{i}_2$ (as illustrated in Fig. 8), three vectors are also modulated. It allows compensating the converter current error $\Delta\boldsymbol{i}_2$ in one control period.

However, in a dynamic state, when the error vector $\Delta\boldsymbol{i}_2$ tail is placed outside the hexagon defined by current derivatives $\boldsymbol{d}_{2i'xxx'}$, one vector is used for the entire control period. In this control mode, it is not possible to compensate the current error $\Delta\boldsymbol{i}_2$ to zero during a single control step. The selection of the generated vector is based on the analysis of the distance between the heads of vectors $\boldsymbol{d}_{2i'xxx'}$ and $\Delta\boldsymbol{i}_2$. The vector that generates the shortest distance is selected. In this way, the smallest error of the $\Delta\boldsymbol{i}_2$ vector is obtained after a control period.

4. Numerical test

Simulation tests were conducted in the Matlab Simulink environment. Parameters of the tested system are presented in Table 1. Internal filter resonance frequencies should be greater than ten times the frequency of grid voltage and less than half the modulation frequency [19]. According to parameters presented in Table 1, the resonant frequencies of the used filter are equal to: $fr_1 = 1.17$ kHz (elements L_1 and C), $fr_2 = 744$Hz (elements L_2 and C) and $fr = 1.39$ kHz.

Table 1
Parameters of the tested circuit used in the numerical test

Parameter	Value
Grid voltage $U_{ph\text{-}rms}$	230 V
Grid frequency f_g	50 Hz
DC link voltage U_{DC}	650 V
Grid side inductance L_1	1.83 mH
Converter side inductance L_2	4.57 mH
Filter capacitance C	10 µF
Sampling time of control circuit T_s	200 µs
Modulation frequency f_m	5 kHz

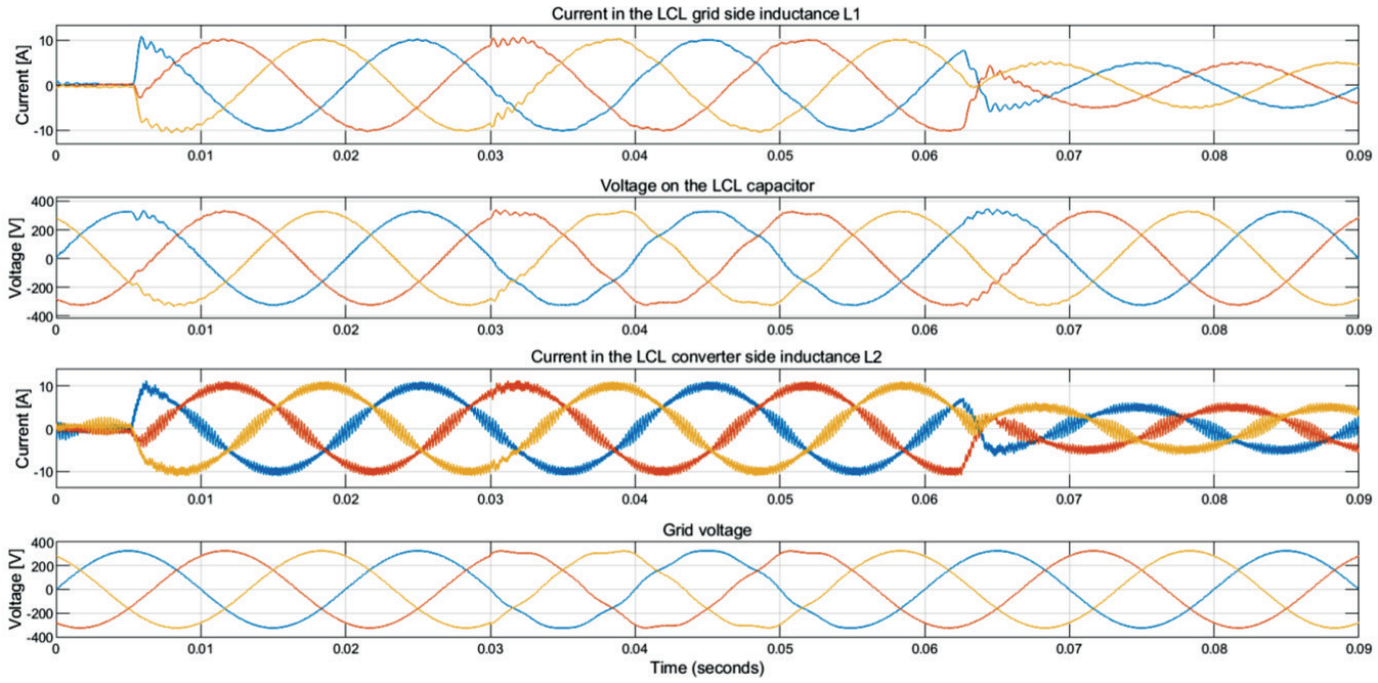

Fig. 9. LCL filter voltages and currents waveforms obtained in the numerical test under various power conditions and setpoint of grid current

The simulation result (Fig. 9) shows how the control system operates both under static and dynamic conditions. At the time 0.05 s the x grid current component was set to 10 A. In the time interval from 0.1s to 0.3 s the measured THD of the grid current is about 0.99%, and the THD of the capacitor voltage is 0.94%. In the next point (0.3 s), a distortion was added to the power grid voltage. Power grid voltage was distorted by the 5^{th} and 7^{th} harmonic (3.00% of fundamental harmonic), i.e., overall grid voltage THD was 4.24%. This results in an increase in the generated grid current THD. Under that condition, for one period of the supply voltage (0.35–0.55 s), the THD of the grid current increased to 3.0%. Also, the THD of the LCL filter capacitor voltage at this time rose to 4.64%. A step-change in x component of the grid current from 10A to −5 A (at 0.625s) leads to perturbation in the filter capacitor voltage. The transient state lasts about 2ms. An overshoot of the filter capacitor voltage is 50 V. Changing the grid current setpoint or rapid change of voltage in the power grid causes minor perturbations in the grid voltage and current. Their amplitude does not exceed 1.5 A in the grid current and 60 V in the filter capacitor voltage during the simulation. The maximal length of the recorded perturbation is 5 ms.

5. Laboratory test

The laboratory test was performed at the same specification as in simulation. The control algorithm was created in a C++ language, and loaded into microprocessor Analog Devices ADSP-21369. The microprocessor is designed to gather all signals from the voltage and current transducers and compute duty cycles for each phase. The generation of gate pulses for transistors in a two-level AC-DC converter is executed in Spartan XC3S400 FPGA.

To obtain a bi-directional current flow from the power grid, a lead-acid battery pack was connected to the DC-link through a DC-DC converter. The tested system is powered by an arbitrary power source California MX30–3Pi. This equipment allows us to conduct tests under different power conditions. Presented time courses were recorded on Tektronix DPO7054C oscilloscope.

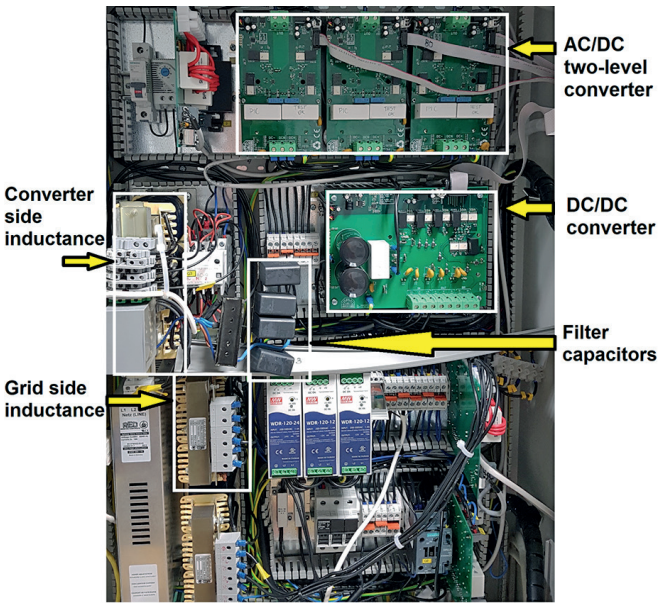

Fig. 10. Hardware configuration of a tested system in a laboratory

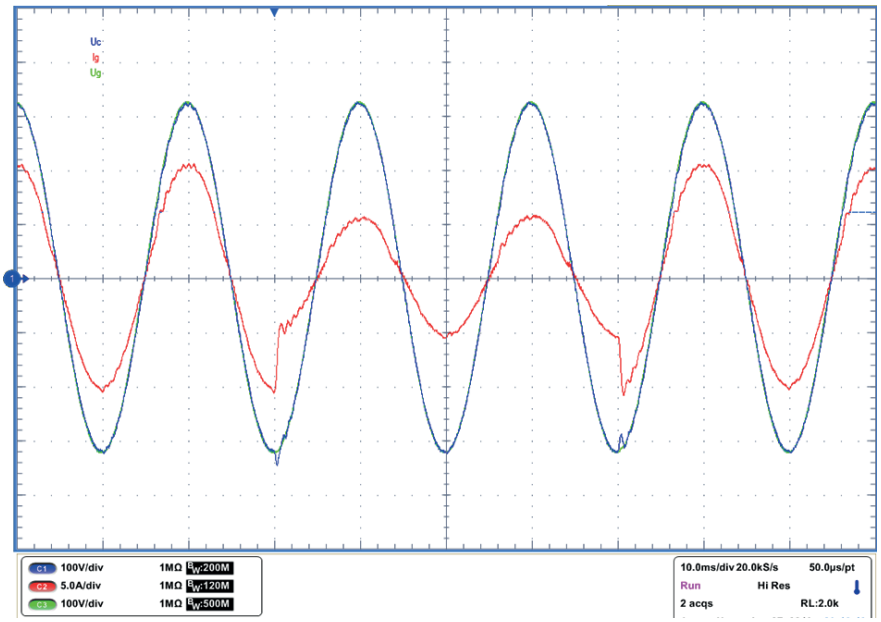

Fig. 11. The grid current (red – 5A/div.), LCL capacitor voltage (blue – 100V/div.), and power grid voltage (green – 100 V/div.) waveforms captured on a tested system under balanced and symmetrical grid voltage. Timebase – 10 ms/div (The green and blue lines overlap)

The measuring of the THD levels in the grid current was conducted in software included with the California power source.

Time courses of voltages and currents in the tested system under sinusoidal and balanced power grid voltage are presented in Fig. 11. The measured grid current THD in steady state is 2.5%. The presented time courses of the grid voltage and filter capacitor voltage are overlapping. This indicates that the algorithm accurately mimics the waveform of the power grid voltage on the filter capacitor voltage. This figure also shows a dynamic state. The dynamic condition changes the x grid current component from 10 A to 5 A and vice versa. At the time of the first transient, the filter capacitor voltage was momentarily increased by 25 V for a time less than 1ms. When the second transient was triggered, a 35 V spike on the capacitor voltage waveform occurs. The voltage increase lasts about 1 ms.

Figure 12 presents a system tested under distorted conditions. The same harmonic distortion was used as in the numerical test, i.e. the 5th and 7th harmonic in the power grid voltage.

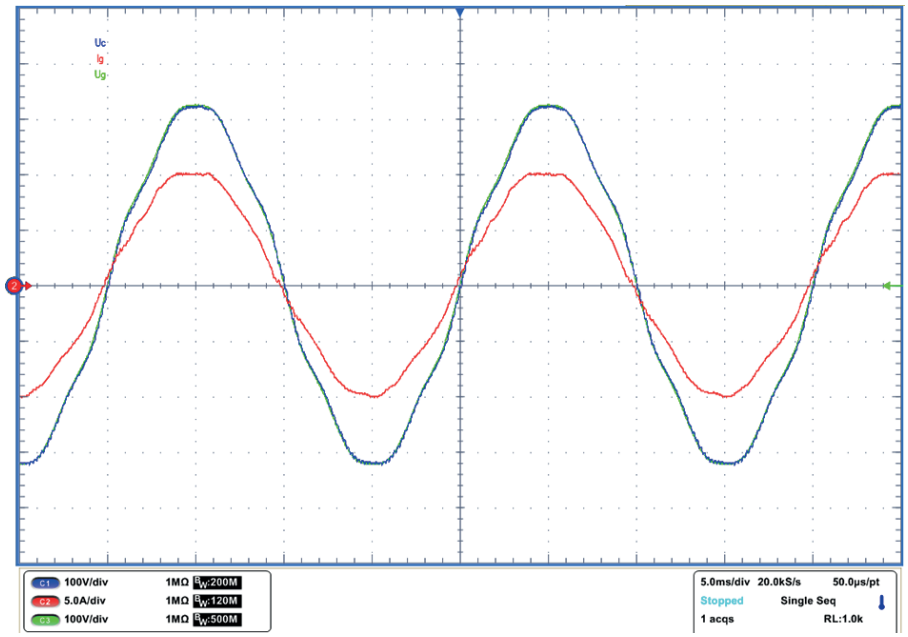

Fig. 12. The grid current (red – 5A/div.), LCL capacitor voltage (blue – 100V/div.), and power grid voltage (green – 100V/div.) waveforms captured on tested system under balanced and distorted grid voltage. Timebase – 10ms/div (The green and blue lines overlap)

The grid current THD amounted to 3.1%. As can be seen, there is no significant increase in the current distortion due to the distorted grid voltage.

When comparing the results of the simulation and laboratory tests, one can note that these results are convergent. In transient states, the simulations very well reflected the momentary voltage changes in the network filter capacitors compared to the tests performed in the real system. However, in a steady state the higher THD of the current in the grid inductance was obtained, which is caused by the limitation of the laboratory hardware equipment (e.g. measurement voltages, currents and processing those signals) and inaccuracies of the model parameters.

6. Conclusions

The proposed control method is ultimately fulfilling the primary assumption, which is sufficient regulation of voltage on the filter capacitors. The presented waveforms confirm that the algorithm is able to effectively reduce the capacitor voltage oscillations caused by the filter resonance, as its shape mimics the shape of the grid voltage in the static condition. This results in a sinusoid, satisfying quality of the grid current. It is worth emphasizing that the assumed purpose of voltage control on the filter capacitor is attained by using only eight available vectors of the two-level converter with low modulation frequency (long control period). The selection of appropriate vectors and their time of use based on the position vectors $\boldsymbol{i}_2$ and $\Delta\boldsymbol{i}_2$ provides precise control over many variables in an LCL filter ($\boldsymbol{i}_1$, $\boldsymbol{i}_2$, $\boldsymbol{u}_c$). The use of space vector modulator results in the presence of characteristic harmonics in the generated current. This approach affects a more comfortable design of the input converter filter. In contrast to nonlinear control methods, the current spectrum is well known. The values of filter elements can be selected directly to suppress the generated current components related to the SVM modulator effectively.

Acknowledgments. The work was supported by the research project WI/WE-IA/1/2019 funded by The Scientific Subsidy of the Polish Ministry of Science and Higher Education.

References

[1] W. El-Khattam and M.M.A Salama, "Distributed generation technologies, definitions and benefits", *Electr. Power Syst. Res.* 71(2) 119–128 (2004).

[2] H.A. Muqeet, A. Ahmad, I.A. Sajjad, R. Liaqat, A. Raza and M.M. Iqbal, "Benefits of Distributed Energy and Storage System in Prosumer Based Electricity Market", *IEEE EEEIC / I&CPS Europe*, Genova, 2019, pp. 1–6.

[3] N. Daryani, K. Zare and S. Tohidi, "Design for independent and self-adequate microgrids in distribution systems considering optimal allocation of DG units", *IET Gener. Transm. Distrib.* 14(5), 728–734 (2020).

[4] V. Narayanan, S. Kewat and B. Singh, "Solar PV-BES Based Microgrid System with Multifunctional VSC", *IET Gener. Transm. Distrib*. 14(5), 728–734 (2020).

[5] D. Kumar and F. Zare, "Harmonic Analysis of Grid Connected Power Electronic Systems in Low Voltage Distribution Networks", *IEEE Trans. Emerg. Sel. Topics Power Electron.* 4(1), 70–79 (2016).

[6] F. Wang, "Flexible operation of grid-interfacing converters in distribution networks: bottom-up solutions to voltage quality enhancement", Technische Universiteit Eindhoven, 2010.

[7] H. Dghim, A. El-Naggar and I. Erlich, "Harmonic distortion in low voltage grid with grid-connected photovoltaic", in *ICHQP*, Ljubljana, 2018, pp. 1–6.

[8] U.P. Yagnik and M.D. Solanki, "Comparison of L, LC & LCL filter for grid connected converter", in *ICEI*, Tirunelveli, 2017, pp. 455–458

[9] H. Cha and T. Vu, "Comparative analysis of low-pass output filter for single-phase grid-connected Photovoltaic inverter", *IEEE APEC*, pp. 1659–1665, Palm Springs, 2010.

[10] P. Channegowda and V. John, "Filter Optimization for Grid Interactive Voltage Source Inverters", *IEEE Trans. Ind. Electron.* 57(12), 4106–4114 (2010).

[11] G.E.M. Ruiz, N. Muñoz and J.B. Cano, "Modeling, analysis and design procedure of LCL filter for grid connected converters", in *PEPQA*, Bogota, 2015, pp. 1–6.

[12] P. Falkowski, K. Kulikowski and R. Grodzki, „Predictive and look-up table control methods of a three-level AC-DC converter under distorted grid voltage", *Bull. Pol. Ac.: Tech*. 65(5), 609–618 (2017).

[13] N. Panten, N. Hoffmann and F. W. Fuchs, "Finite Control Set Model Predictive Current Control for Grid-Connected Voltage-Source Converters With LCL Filters: A Study Based on Different State Feedbacks", *IEEE Trans. Power Electron.* 31(7), 5189–5200 (2016).

[14] M. Liserre, A. Dell'Aquila and F. Blaabjerg, "Stability improvements of an LCL-filter based three-phase active rectifier", in *IEEE PESC*, vol. 3, Cairns, 2002, pp. 1195–1201.

[15] M.M. Aghdam, L. Li and J. Zhu, "Comprehensive study of finite control set model predictive control algorithms for power converter control in microgrids", *IET Smart Grid* 3(1), 1–10 (2020).

[16] X. Zhang, L. Tan, J. Xian and H. Zhang, "Three vector complete model predictive control for three-phase grid-connected inverters with LCL filter", *ICIEA*, Wuhan, 2018, pp. 14701475.

[17] R. Mahmud and M.A. Rahman, "Proportional Integral Resonant Current Controller for Grid Connected Inverter in Distributed Generation System using SVPWM Technic", *IC4ME2*, Rajshahi, 2018, pp. 1–4.

[18] A. Godlewska, R. Grodzki, P. Falkowski, M. Korzeniewski, K. Kulikowski and A. Sikorski, "Advanced Control Methods of DC/AC and AC/DC Power Converters—Look-Up Table and Predictive Algorithms", in *Advanced Control of Electrical Drives and Power Electronic Converters*, Ed. J. Kabziński, vol. 75, pp. 221–302 Springer International Publishing, 2017.

[19] F. Liu, X. Zhang, C. Yu, Z. Shao, W. Zhao and H. Ni, "LCL-filter design for grid-connected three-phase PWM converter based on maximum current ripple", *IEEE ECCE*, Melbourne, 2013, pp. 631–635.